International Journal of Remote Sensing

ISSN: 0143-1161 (Print) 1366-5901 (Online) Journal homepage: https://www.tandfonline.com/loi/tres20

Long-term skill assessment of SeaSonde radar-derived wave parameters in the Galician coast (NW Spain)

P. Lorente, A. Basañez Mercader, S. Piedracoba, V. Pérez-Muñuzuri, P. Montero, M.G. Sotillo & E. Álvarez-Fanjul

INTERNATIONAL JOURNAL OF REMOTE SENSING
2019, VOL. 40, NO. 24, 9208–9236
https://doi.org/10.1080/01431161.2019.1629714

Taylor & Francis
Taylor & Francis Group

Check for updates

Long-term skill assessment of SeaSonde radar-derived wave parameters in the Galician coast (NW Spain)

P. Lorente[a], A. Basañez Mercader[b], S. Piedracoba[c], V. Pérez-Muñuzuri[b], P. Montero[d], M.G. Sotillo[a] and E. Álvarez-Fanjul[a]

[a]Puertos del Estado, Madrid, Spain; [b]Grupo de Física No-lineal, Universidad de Santiago de Compostela, A Coruña, Spain; [c]Centro Tecnológico del Mar, CETMAR, Vigo, Spain; [d]Instituto Tecnolóxico para o Control do Medio Mariño de Galicia, INTECMAR, Vilagarcía de Arousa, Spain

ABSTRACT

A long-term multi-parameter skill assessment of a 5-MHz Coastal Ocean Dynamics Applications Radar (CODAR) SeaSonde High-Frequency radar (HFR) network deployed along the Galician Coast (NW Iberian Peninsula) was attempted for 2014–2016. To this aim, wave estimations from two HFR sites, obtained directly by the CODAR radar proprietary software, were independently validated against hourly in situ observations from two moored buoys for two different periods. The accuracy assessment of significant wave height (H_s) revealed a consistent agreement with Pearson´s correlation coefficients (r) above 0.75 and normalized root mean squared errors below 0.4. An overall slight overestimation of H_s radar estimations was evidenced, likely due to spurious contributions to the directional spectra. The seasonal analysis revealed that the performance of this low mono-frequency radar was more precise for high-sea states during wintertime, whereas the quality and availability of radar data decreased under summer less energetic conditions, in accordance with previous works. In the case of the centroid wave period, HFR performance was consistent through the different years, with r values emerging in the range of 0.61–0.74. The directional accuracy was moderately good, with NW and W-NW as predominant sectors. Despite r values above 0.74, a tendency for CODAR HFR-derived incoming mean wave direction to be aligned more perpendicular to the coast compared to offshore in situ data was also observed. Furthermore, the relationship between the North Atlantic Oscillation (NAO) and HFR wave estimations was explored. A subtle but statistically significant connection was found, with H_s and centroid wave period being positively correlated with NAO daily index. Complementarily, the skill of the Galician HFR system was evaluated under positive and negative NAO conditions in order to elucidate whether the radar accuracy is or is not NAO-phase dependent. No substantial differences could be found for each of the three parameters analysed as HFR accuracy remained mostly unaffected by swings in the NAO index. Finally, it can be concluded that properly treated CODAR radar-derived wave estimations can be potentially employed for operational coastal monitoring across a wide range of sea states.

ARTICLE HISTORY
Received 3 June 2018
Accepted 21 April 2019

CONTACT P. Lorente plorente@puertos.es Puertos del Estado, Madrid, Spain

1. Introduction

Single-point in situ marine devices present some instrumental limitations in terms of spatial resolution and areal coverage and are also subject to costly repairs. For this reason, noticeable efforts have been devoted over the last decades to the development of alternative land-based remote-sensing techniques such as High-Frequency radars (HFR). This consolidated cost-effective technology is based on measurements of the radiowave-backscattered signal from ocean surface gravity waves in the 3–30 MHz range of the electromagnetic spectrum along with the subsequent analysis of the Doppler-shifted echoes (Crombie 1955; Prandle 1991). HFR systems have proved their capability to provide reliable directional wave and wind information along with surface current vector maps in the near real time for a variety of temporal scales and spatial resolutions (Graber and Heron 1997; Fernandez et al. 1997; Barrick 1977; Barrick, Evans, and Weber 1977). As a consequence, the HFR network has grown worldwide rapidly, becoming an essential component of coastal ocean observation systems (James et al. 2019; Rubio et al. 2017; Quentin et al. 2017).

According to the methodology used to isolate the ocean sector where scattering occurs, HFR systems can be differentiated into two major types: i) beam-forming radars, which electronically point linear phased arrays of receive antennas toward a sector of the ocean; and ii) direction-finding radars, which measure the return signal continuously over all angles, exploiting the directional properties of a collocated three-element receive antennae system and the Multiple Signal characterization (MUSIC) algorithm (Schmidt 1986) in order to determine the direction of the incoming signals. Whereas Pisces (Shearman and Moorhead 1988) belongs to the first type, Coastal Ocean Dynamics Applications Radar (CODAR) systems (Barrick, Evans, and Weber 1977) and Ocean State Monitoring and Analysing Radar (OSMAR-S) systems (Zhou, Roarty, and Wen 2015) are direction-finding radars. On the other hand, the WEllen RAdar (WERA) systems (Gurgel et al. 1999) has both phased-array and direction-finding options.

Robust surface current measurements can be derived from the Doppler shift of the dominant first-order peak in the radar echo spectrum (Crombie 1955). Wind measurement requires a mix of first- and second-order information (Wyatt 2018; Wyatt et al. 2006). The directional wave spectrum and derived parameters such as local significant wave height, centroid wave period and mean wave direction can be determined from the weaker second-order sea-echo Doppler spectrum by adopting two main approaches: full integral inversion or fitting with a model of ocean wave spectrum (Lipa and Nyden 2005). A variety of inverse techniques have been developed over the last years (Barrick 1977; Wyatt 1990; Hisaki 2006). Direction-finding HFR systems provide wave measurements at specific ranges (assuming the homogeneity over the whole of each range), whereas phased-array HFR systems estimate wave maps with similar spatio-temporal resolution as for current measurements.

The second-order scattering-based methods significantly rely on the echo quality which varies with sea state (Wyatt et al. 2005). Since the wave data is dependent upon the occurrence of both Bragg and larger surface gravity waves, there is a minimum threshold for sea states in which reliable wave parameters can be determined. Below such sensitivity threshold, the lower-energy second-order spectrum is closer to the noise floor and more likely to be contaminated with spurious contributions that might result in wave height overestimation or limited temporal continuity in wave measurements (Lipa and Nyden 2005; Tian et al. 2017; Lipa et al. 2018). During extreme weather events, there is also a limiting factor for HFR accuracy as the wave height increases and exceeds the saturation limit defined (on an inverse proportion) by the radar transmit frequency. If the radar spectrum saturates, the first-order peak merges with the second-order one and interpretation of the spectra becomes impossible with existing methods (Forney, Roarty, and Glenn 2015). In this context, recent efforts have focused on the improvement of multiscale wave height estimation for highly variable sea states by using dual-frequency HFR systems (Wyatt and Green 2009; Tian, Wen, and Zhou 2014) or by extracting wave information directly from the first-order Bragg peaks (Zhou and Wen 2015) in order to overcome the wave height limitation at single-frequency and to better measure low and moderate waves, respectively.

Wave measurements derived from HFR have a broad range of potential applications and can be used as input data for numerical models validation (Lorente et al. 2017; Saviano et al. 2017) or assimilation into wave models such as Simulating WAves Nearshore (SWAN; Siddons, Wyatt, and Wolf 2009) or high-resolution coastal Wavewatch III (Waters et al. 2013). They can be also employed to determine a reliable figure for available resource with regard to wave energy harvesting (Atan et al. 2016a; Ramos, Graber, and Haus 2009) or the analysis of extreme wave height events (Atan et al. 2015, 2016a; Lorente et al. 2018).

In order to infer how much confidence can be placed in wave parameters provided by the present CODAR SeaSonde HFR system, their consistency and accuracy must be assessed by means of rigorous validation studies. Previous experiments, listed in Table 1, included comparisons against in situ wave measurements over a variety of regions (Alfonso, Álvarez-Fanjul, and López 2006; Long et al. 2011; Toro et al. 2014; Gómez et al. 2015; Atan et al. 2015; López, Conley, and Greaves 2016; Orasi et al. 2018). Regardless of both the manufacturer and the methodology used to determine wave parameters, the positive contribution of commercial HFR systems to retrieve realistic wave information has been unequivocally proven. The primary goal of this

Table 1. Review of previous studies about validation of High-Frequency radar (HFR) derived wave height (H_s) data against in situ observations. The manufactures (HFR type) and operating frequency are provided. Skill metrics obtained during the studied period included root mean square error (RMSE) and Pearson´s correlation coefficient (r). Note that in the case of the phased-array systems mentioned here a number of different inversion methods have been used.

					Skill metrics (H_s)	
Reference (year)	Brand	HFR type	Freq. (MHz)	Period (months)	RMSE (cm)	r
Alfonso, Álvarez-Fanjul, and López (2006)	CODAR	Direction-finding	4.86	3	69–89	0.89–0.94
Wyatt et al. (2006)	Pisces	Phased array	5–15	3	27–49	0.72–0.90
Wyatt, Green, and Middleditch (2011)	Pisces	Phased array	7–12	4	45	0.91
Long et al. (2011)	CODAR	Direction-finding	12–13	15–26	46–77	0.85–0.91
Toro et al. (2014)	WERA	Both	16.3	3	24–39	0.73–0.95
Gómez et al. (2015)	WERA	Both	12	6.5	40–69	0.78–0.92
Atan et al. (2015)	CODAR	Direction-finding	25	3	29–40	0.69–0.84
López, Conley, and Greaves (2016)	WERA	Both	12	5	29–52	0.88–0.95
Zhou, Roarty, and Wen (2015)	OSMAR-S	Direction-finding	13	3	77–93	0.67–0.74

paper is to conduct a long-term skill assessment of CODAR SeaSonde HFR-derived wave parameters in the Galician coast (NW Iberian Peninsula, Figure 1). This region is strongly influenced by mid-Atlantic low-pressure systems with periodic passage of storms that give rise to severe sea states. Therefore, a comprehensive characterization of the wave field is critical for both marine safety and coastal engineering. To this aim, two independent validation exercises with two HFR sites have been performed for different periods using as benchmark quality-controlled hourly in situ wave measurements provided by Silleiro and Vilán moored buoys, hereafter referred as to B1 and B2, respectively (Figure 1(a)). The purpose of this paper is not to intercompare the two HFR sites but rather to evaluate the accuracy at each site on a seasonal basis since low mono-frequency radar systems are expected to be more adequate to properly monitor winter high waves than summer low-moderate waves, as previously reported by Wyatt and Green (2009) and Tian, Wen, and Zhou (2014). Within this context, a detailed quantification of the precision loss is highly required.

The present study builds on previous validation works carried out with the HFR network (Figure 1(b)) operated by Puertos del Estado (Lorente, Piedracoba, and Álvarez-Fanjul 2015; Lorente et al. 2016). Whilst a preliminary 4-month (November 2005 – February 2006) accuracy assessment of HFR-derived wave data was conducted by Alfonso, Álvarez-Fanjul, and López (2006), the present research considers a much longer period (2014–2016) and provides a deeper insight. To our knowledge, only a few studies have previously dealt with long time series of HFR-derived wave parameters (Saviano et al. 2019; Atan et al. 2016a; Long et al. 2011; Wyatt et al. 2006). Within this context, an additional objective is to assess the annual and seasonal wave characteristics and the related temporal variability under different sea states and coastal configurations.

The wintertime variability of the North Atlantic cyclonic activity is primarily modulated by the North Atlantic Oscillation (NAO). Since the influence of NAO on waves along the Atlantic

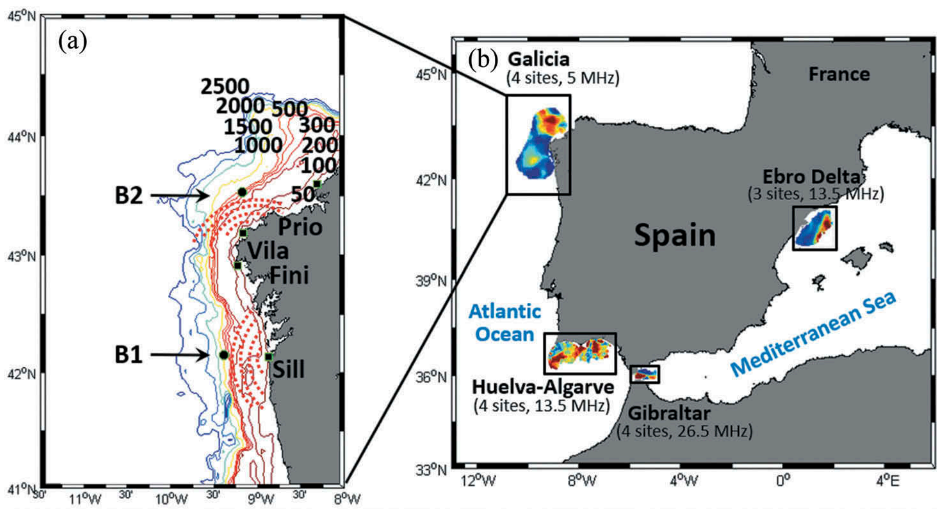

Figure 1. (a) General area of study and HF radar coverage area: cells emerge concentrically from each radar site. Locations of Silleiro buoy (B1, 45 km far from shore), Vilán buoy (B2, 37 km far from shore) and four radar sites (Sill, Fini, Vila and Prio) are marked with a filled dot and squares, respectively. Bathymetric contours show depths at 400 and 1500 m. (b) HF coastal radar network managed by Puertos del Estado, INTECMAR and Instituto Hidrográfico de Portugal.

coast of Europe is particularly strong in wintertime (Atan, Goggins, and Nash 2016b; Martínez-Asensio et al. 2016), this relationship has been also explored by comparing the daily NAO index with remote-sensed HFR wave estimations. While the NAO has a major impact on northern latitudes, its influence on the inter-annual variations of wave height is more subtle in the Iberian Peninsula (Castelle et al. 2017). Therefore, capturing the NAO signal in HFR-derived measurements is particularly challenging in the Galician coast. In this line, it is also relevant to evaluate if HFR performance is NAO-phase dependent or by contrast its overall accuracy remains unaffected by swings in the NAO index.

2. Instrumentation and methods

2.1. Buoy setup

The HFR footprint overlooks two deep ocean Seawatch buoys operated by Puertos del Estado since 1998 and moored in the north-western waters of the Iberian Peninsula (Figure 1(a)), just in the edge of the continental shelf: B1 (42°7´12´´N, 9°26´24´´W, 600 m depth) and B2 (43°30´N, 9°13´12´´ W, 386 m depth).

Hourly-averaged quality-controlled measurements of significant wave height (H_s), wave period at spectral peak (or peak period), and mean wave direction were provided by a directional Waverider sensor. The quality control, defined by the CMEMS in situ team (Copernicus Marine In situ Team 2017), was based on a battery of automatic checks performed in real time to flag and subsequently filter inconsistent values. Some of the tests are listed in Table 2.

Finally, it is also worthwhile mentioning the intrinsic uncertainties related to the in situ sensors: the instrumental error was below 0.5% of measured H_s values after calibration, according to the manufacturer. B1 presented some occasional gaps in the wave data supply during spring-summer 2015 (Figure 2(a)). The rest of the 3-year study period the data provision was almost 100%. B2 buoy had a more erratic performance in terms of data availability, which generally fluctuated between 60%-100% during 2014 and 2015 years (Figure 2(b)).

2.2. Climate indices

The NAO index refers to changes in the atmospheric sea level pressure difference between the Azores and Iceland (Hurrel 1995). Daily climate indices associated with the NAO and spanning the 3-year period (2014–2016) were freely downloaded from the National Oceanic

Table 2. Automatic quality-control checks defined by the Copernicus Marine In situ Team and performed in real time to in situ wave measurements.

Check	Description
Global range test	Gross filter based on observed values for waves. It needs to accommodate all of the expected extremes encountered in the study region.
Spike test	Based on the difference between sequential measurements. For the significant wave height, wave period and wave peak period, a value is flagged when the difference exceeds 3 m, 4 s and 15 s, respectively, for the Atlantic ocean.
Stuck value test	A wave parameter should not remain in the same value for more than 12 hours with more than 50% of data not null and valid.
Rate of change in time	Based on the difference between the current value with the previous and next ones.

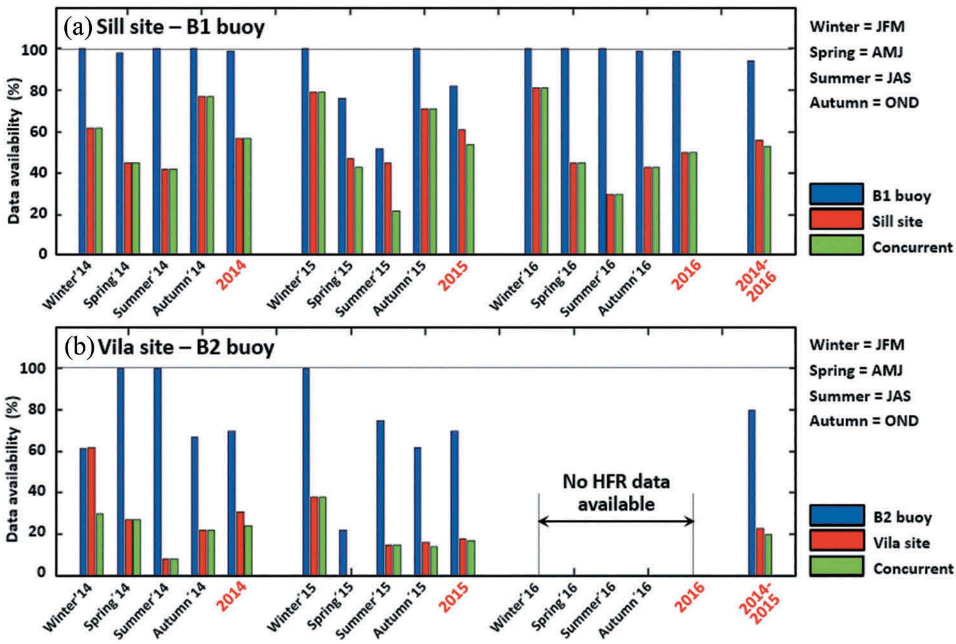

Figure 2. (a) Data supply (in percentage) of significant wave height on a quarterly and annual basis during 2014–2016: B1 buoy availability (blue column), HFR availability (Sill site, red column) and concurrent time periods (green column). (b) Data supply (in percentage) of significant wave height on a quarterly and annual basis during 2014–2015: B2 buoy availability (blue column), HFR availability (Vila site, red column) and concurrent time periods (green column).

and Atmospheric Administration (NOAA) Climate Prediction Centre (http://www.cpc.ncep.noaa.gov/products/precip/CWlink/pna/nao.shtml). The daily NAO index is constructed by projecting the daily (00Z) 500 mbar height anomalies over the Northern Hemisphere onto the loading pattern of the NAO and then normalized by the standard deviation of the monthly NAO index from 1950 to 2000.

2.3. High-frequency radar set up

The CODAR SeaSonde long-range 5-MHz HFR system used in this work was deployed in Galicia in November 2004. It is composed of four sites from south to north (Figure 1(a)): Silleiro (Sill) and Finisterre (Fini), operated by Puertos del Estado; Vilán (Vila) and Prior (Prio), operated by Instituto tecnoloxico para o control do medio mariño (INTECMAR). Each single radar site is configured to estimate both radial currents moving towards or away from the site and waves. Each site operates at a central frequency of 4.86 MHz, providing current vectors which are representative of the upper 2 m of the water column. The maximum horizontal range is set to 200 km, and the nominal range and angular resolutions are 5.1 km and 5°, respectively.

HFR wave parameters included significant wave height, centroid wave period and mean wave direction. Such data were retrieved from five individual range cells, 5.1 km wide, which extended radially from an origin at the onshore radar site of Sill –42.°6´N, 8°53´24´´W- (Vila –43°9´36´´N, 9°12´36´´W-) to a distance 25.5 km offshore. As previously stated, homogeneity over the whole of each range is assumed in CODAR Seasonde HFR systems.

The outermost HFR radar range cell (cell 5) of Sill and Vila radar sites (Figure 1(a)) was selected to perform an independent comparison against B1 and B2 buoys, respectively, as it presented the highest percentage of captured data. Since B1 (B2) buoy is 45 (37) km from shore, we can derive that remote-sensed wave estimations are representative of a region 20 (12) km from the B1 (B2) buoy, setting up the context for the discussion of results. The wave parameters used in this study, based on 30 min averaged backscatter data, were obtained directly by the CODAR radar proprietary software (SeaSonde Radial Suite: Release 6, update 5) which performs a least squares fitting technique between the second-order radar spectrum and a Pierson-Moskowitz with cardioid directional function model. Wave data were collected from 1 January 2014 to 31 December 2016 (2015) in the case Sill (Vila) site. HFR data were subsequently subsampled at 60-min interval in order to provide consistency in the temporal resolution of the data for validation and analysis. In this framework, the quality control used for the in situ wave observations was also applied to CODAR HFR-derived estimations.

Wave data supply from Sill site was irregular during 2014–2016 (56%, Figure 2(a)), with a maximum (minimum) around 80% (30%) during wintertime (summertime), giving evidence of the existence of a minimum threshold for sea states in which reliable wave parameters can be derived. The 3-year time-averaged data availability was around 57% for this site. In the case of Vila site, data provision was significantly limited during 2014–2015, ranging from 5% (summer 2014) to 60% (winter 2014), with a rather poor 20% of overall availability for a 2-year study period (Figure 2(b)). It is worth mentioning that during part of the study period, this radar site operated freely as it could not be properly maintained due to severe economic restrictions. In addition, its radar band was occasionally congested with industrial interferences, which constituted the main source of error and gave rise to noisy HFR wave estimations, as observed in early February 2014 (Figure 3(b)).

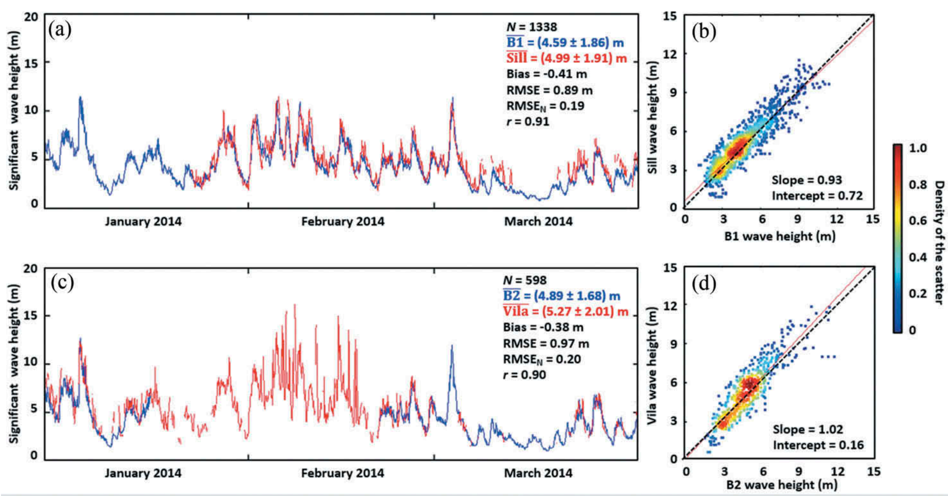

Figure 3. Three-month validation of hourly significant wave height estimations provided by High-Frequency radar (red line) against in situ observations (blue line). (a-b) Sill radar site against B1 buoy: time series comparison and best linear fit (red line) of scatter plot, respectively; (c-d) Vila radar site against B2 buoy: time series comparison and best linear fit (red line) of scatter plot, respectively. Skill metrics are gathered on the right. N represents the number of hourly observations. Dashed black lines represent the result of perfect agreement with slope 1.0 and intercept 0.

2.4. Wave parameters validation

The HFR-buoy agreement has been evaluated by means of time series comparison and the subsequent computation of a set of statistical metrics: histograms, bias, Root Mean Squared Error (RMSE), RMSE normalized by the mean of the observed data ($RMSE_N$), Pearson´s correlation coefficients (r), quantile–quantile (QQ) plots, the best linear fit of scatter plots and wave roses. All correlations cited in the manuscript were significant at the 90% confidence level (Emery and Thompson 2001, p. 253) unless otherwise indicated. Annual and quarterly results have been gathered in Taylor diagrams (Taylor 2001), which provide a concise statistical summary of the accordance between both data sets. In terms of characterizing wave height events, we adopted the criterion defined by Atan et al. (2015) where high (extreme) H_s events occur between the 90th and 99th (99th and 100th) percentiles; hereafter, referred to as P90–P99 (P99–P100), respectively. In order to conduct the preliminary skill assessment, the radar range cell geographically closest to each buoy location was selected for each HFR site (Figure 1(a)) and hourly estimations at the selected Sill (Vila) cell were compared with in situ data from B1 (B2) moored buoy. The 3-month wintertime (JFM) comparisons reveal the significant skill of both Sill and Vila radar sites (especially the former), with moderate $RMSE_N$ (around 0.20) and r values above 0.90 (Figure 3). The HFR system appears to properly capture the main peaks of H_s (above 10 m). Equally, the slope and intercept values derived from the best linear fit are close to 1 and 0, respectively. According to these preliminary results, which are in line with previous validations reported elsewhere (Long et al. 2011; Atan et al. 2015; López, Conley, and Greaves 2016), we can state that HFR performance seems to be rather consistent and within tolerance ranges. Therefore, it might act as a useful ancillary tool, especially in locations where in situ measuring devices cannot be deployed (such as harbour entrances) or when in situ wave observations are temporarily unavailable, as occurred with the B2 buoy during February 2014 (Figure 3(b)).

3. Results and discussion

3.1. Significant wave height

In this section, a long-term skill assessment has been conducted to infer the overall accuracy of CODAR HFR-derived estimations of H_s. There is a reasonable similarity among Sill radar site and B1 buoy hourly observations for the selected 3-year period (Figure 4(a)). This statement is supported by the skill metrics gathered on the right side, with an $RMSE_N$ of 0.27 and r above 0.8. The main wintertime H_s peaks, which lie in the range 6–12 m, are fairly well captured despite some occasional and time-limited gaps in the time series. According to the negative bias, HFR seems to slightly overestimate the wave height across a wide range of sea states.

The 2-year time series comparison of Vila site and B2 buoy reveal significant gaps in the data provision (Figure 4(b)), with only a 20% of available concurrent data (Figure 2 (b)). The radar site exhibits some spike-like fluctuations and an H_s overestimation in high sea-states, especially during February 2014 and winter 2014–2015, as reflected by higher than expected RMSE and $RMSE_N$. Although r value is still satisfactory (0.75), it is reasonable to assume that the discriminating algorithm defined in the quality-control protocol (Table 2) should impose tighter thresholds for this radar site. However, the main

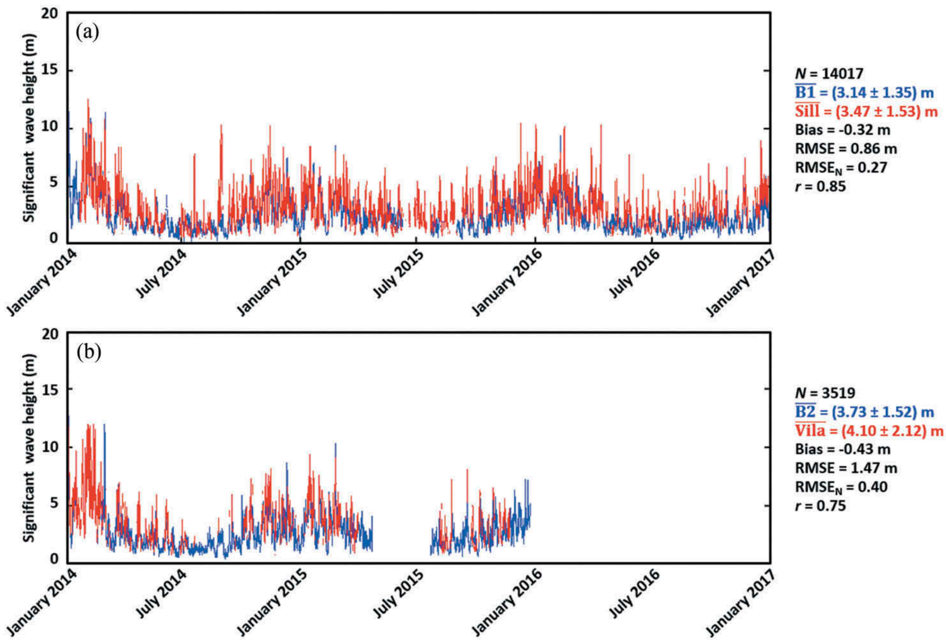

Figure 4. Validation of hourly significant wave height estimations provided by High-Frequency radar (red line) against in situ observations (blue line) for the period 2014–2016. (a) Sill site against B1 buoy; (b) Vila site against B2 buoy. Skill metrics are gathered on the right. N represents the number of hourly observations.

drawback lies with the potential removal of accurate data and the reduction of the already time-limited data availability. Notwithstanding, the r values obtained for both radar sites are in accordance with previous results reported in the literature (Table 1) and also in line with the skill metrics described by Alfonso, Álvarez-Fanjul, and López (2006) with the same HFR system, taking into account that here a longer time period was considered.

Additional statistical indicators have been computed and illustrated in Figure 5. A histogram, showing the number of hourly H_s observations per class interval (Figure 5 (a)), exhibits a Rayleigh-like distribution clustered around 3.5 m mean (Sill site) and slightly shifted to lower values in the case of B1 buoy (3.14 m). Both datasets show similar positive skew and variability, with the standard deviation emerging in the range 1.35–1.53 m for the 2014–2016 period. The results derived from the best linear fit of scatter plot show that the slope is close to 1 and the related coefficient of determination R^2 (0.73) is significantly high (Figure 5(b)). Based on the QQ plot (Figure 5(c)), it can be concluded that Sill wave height estimations are consistent despite the slight overestimation observed for high-sea states, especially for extreme H_s events (99th–100th percentiles).

The 2-year comparison of Vila site and B2 buoy wave height estimations shows similar results for the histogram (Figure 5(d)). The scatter presents higher dispersion and lower (but still statistically significant) R^2 (0.56), despite the robust parameters derived from the best linear fit: the slope and intercept are close to 1 and 0, respectively (Figure 5(e)).

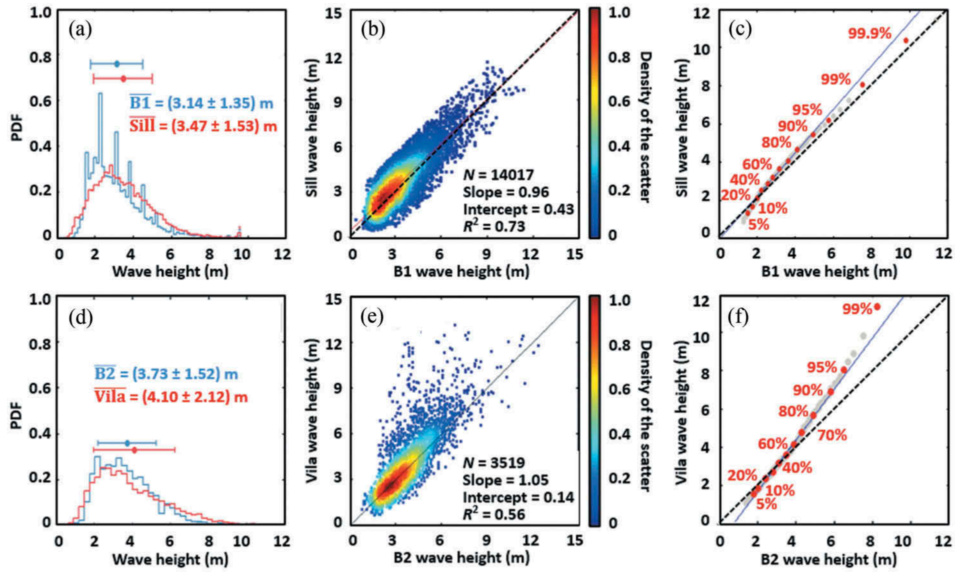

Figure 5. Histogram, best linear fit (red line) of scatter plot and QQ plot of significant wave height: (a-c) Sill radar site against B1 buoy, for the period 2014–2016. (d-f) Vila radar site against B2 buoy, for the period 2014–2015. In the QQ plot, 5–99.9% quantiles were established (red-filled dots). Dashed black lines represent the result of the perfect agreement with slope 1.0 and intercept 0.

Finally, the overall HFR overestimation of wave height events above percentile 80 is clearly evidenced in the QQ plot presented in Figure 5(f).

Since CODAR long-range HFR systems (such as the 5-MHz one used here) do not face problems related to radar spectral saturation during storm peaks, a plausible cause for the detected overestimation in H_s measurements could lie in the assumptions made in the inversion method. The Pierson-Moskowitz fit-to-spectrum model has demonstrated its validity to describe unimodal energy spectra in wind-dominated seas and also in swell-dominated seas (Long et al. 2011; Orasi et al. 2018), while there is scientific evidence this can be different under some combination of bimodal sea-states or when winds blow from land (Lipa et al. 2018). Therefore, the use of an unimodal model under some combination of bimodal sea states might result in significant overestimation of the wave height when the swell is present. In this context, it seems reasonable to suspect that complex met-ocean conditions (such as multimodal sea-states) can impact in uncertainties related to HFR wave estimations. Moreover, the assumption of homogeneity over the whole of each circular range cell in CODAR Seasonde HFR systems could also partially explain the differences detected due to relevant bathymetric variations in coastal areas.

In addition, a portion of the discrepancies observed in H_s measurements in this tidally dominated region could be also partially attributed to the hydrodynamic modulations of waves by periodic underlying currents. Barrick and Lipa (2015) reported inertial oscillatory modulations in both the Galician HFR and B1 buoy H_s measurements, the latter being in phase but weaker than those from the radar. In this context, Lipa et al. (2014) had previously described the significant tidally forced modulation of wave parameters (including wave period and direction) at high latitudes, becoming strongest when tidal currents and waves oppose each other. The waves-current interaction remains as a subject for future investigations.

On the other hand, shallow water is known to impact on radar sea-echo by increasing the second-order spectral energy (relative to the first-order) and decreasing the saturation limit on wave height as water depth decreases (Lipa et al. 2008). For a radar transmit frequency of 5 MHz (the case here studied) the depth at which shallow water effects become significant is 35 m. In this study, the outermost HFR range cell selected was 25.5 km offshore from the coast (Figure 1(a)), far enough to ensure the assumption of deep water is adequate.

Taylor diagrams provide a concise statistical summary of how closely hourly HFR-derived H_s estimations match with in situ observations (red-filled squares), considered here as the reference points of perfect agreement (Figure 6). According to the annual skill metrics, HFR sites performance is consistent, with annual *r* values above 0.8 and RMSE below 80 cm (Figure 6(a)) and slightly better skill metrics for 2014 than for the rest of years considered. The analysis on a quarterly basis reveals interesting seasonal differences: the best skill metrics are recurrently obtained in winter and autumn when severe weather episodes usually take place (Figure 6(b)). As previously mentioned, in low sea states the second-order spectrum of this low-operating frequency HFR is closer to the noise floor. This fact explains the lower than average HFR data availability (Figure 2) and accuracy (Figure 6(b)) during summertime for both Sill and Vila radar sites. Therefore, a multi-frequency HFR with the capability of switching transmit frequency from 5 to 13 MHz could enhance the measuring performance of widely changing H_s, particularly for low and moderate wave heights (Tian, Wen, and Zhou 2014; Chen et al. 2013; Wyatt, Green, and Middleditch 2011; Wyatt and Green 2009; Lipa and Nyden 2005).

The seasonal features of the wave field have been also assessed by means of the combined use of in situ and remote-sensed wave estimations. Table 3 summarizes the time-averaged statistical information and percentiles used in this study. Winter is

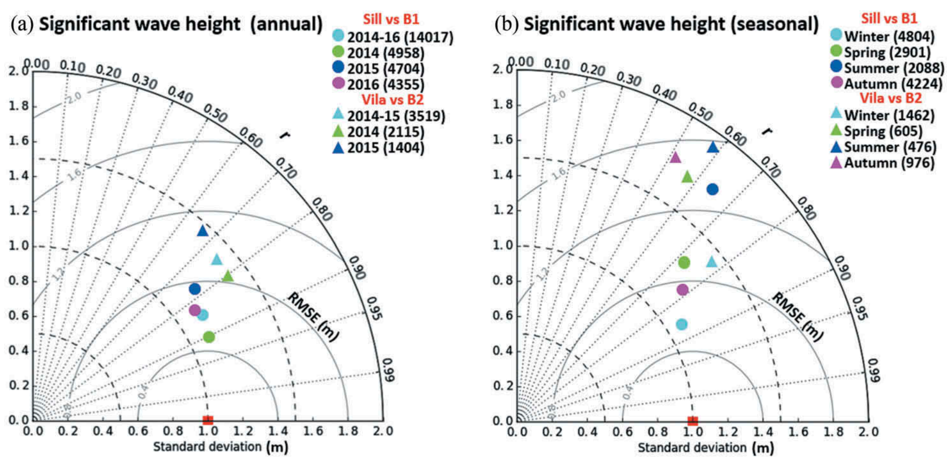

Figure 6. (a) Annual and (b) seasonal Taylor diagrams of significant wave height derived from the comparison of Sill (Vila) radar site against B1 (B2) buoy for the period 2014–2016 (2015–2016).

Table 3. Quarterly statistical metrics of significant wave height obtained for each instrument for the periods 2014–2016 (B1 and Sill) and 2014–2015 (B2 and Vila). *N*, SD, P90 and P99 represent the number of hourly observations, standard deviation and percentiles 90 and 99, respectively.

Season	Instrument	*N*	Mean (m)	SD (m)	P90 (m)	P99 (m)
Winter (J-F-M)	**B1 buoy**	4804	3.94	1.52	5.98	8.91
	Sill site	4804	4.23	1.66	6.35	9.39
	B2 buoy	1462	4.14	1.68	6.21	9.49
	Vila site	1462	4.59	1.71	6.97	9.89
Spring (A-M-J)	**B1 buoy**	2901	2.37	0.76	3.40	4.69
	Sill site	2901	2.56	0.99	3.89	5.21
	B2 buoy	605	2.32	0.67	3.16	3.87
	Vila site	605	2.61	0.91	3.91	5.20
Summer (J-A-S)	**B1 buoy**	2088	2.07	0.59	2.81	4.1
	Sill site	2088	2.43	0.97	3.73	4.97
	B2 buoy	476	1.55	0.50	2.23	2.7
	Vila site	476	2.18	0.67	2.99	4.15
Autumn (O-N-D)	**B1 buoy**	4224	3.30	1.07	4.80	6.33
	Sill site	4224	3.72	1.29	5.50	7.11
	B2 buoy	976	3.22	1.09	4.69	5.68
	Vila site	976	3.53	1.02	4.81	6.24

characterized by H_s around 4 m and presents the highest variability, with the standard deviation above 1.5 m. On average, wave height events in Galicia are defined as high (extreme) when H_s exceeds 6.3 (9.4) m. During autumn high-sea states were also observed, with mean H_s and standard deviation around 3.5 m and 1 m, respectively. By contrast, spring and summer are defined by moderate wave height episodes, with H_s emerging in the range 1.55–2.61 m and the related standard deviation is below 1 m.

3.2. Wave period

Since CODAR SeaSonde HFR systems output a period that represents the centroid of the model being fitted to the second-order Doppler spectrum, when comparing it against in situ measurements, the SeaSonde´s centroid period falls in all cases between the buoy ´s dominant and average period (Long et al. 2011). This fact is relevant to properly interpret the results obtained from the long-term validation of these HFR-derived period estimations, as buoy peak period data were used in this work.

There is a reasonable similarity between Sill radar site and B1 buoy for the period 2014–2016, as illustrated by an $RMSE_N$ and *r* values of 0.17 and 0.65, respectively (Figure 7(a)). According to the positive bias, HFR centroid period estimations are lower than peak period in situ measurements, as previously mentioned. The 2-year time series comparison of Vila site and B2 buoy shows again considerable gaps in the data provision, some spike-like fluctuations and lower periods during summertime (Figure 7(b)); Nevertheless, the *r* value is moderately high (0.69) and the $RMSE_N$ is low (0.25).

Complementary skill indicators are depicted in Figure 8. The histogram of hourly wave period estimations per class interval reveals the discrete distribution of values provided by B1 buoy, rather symmetrical, centred around 12 s and slightly shifted to higher values (Figure 8(a)). HFR-derived centroid period estimations present a continuous statistical distribution, similar to B1 in terms of mean value (11.38 s) and standard deviation (2.04 s) but, as expected, shortened for the highest wave periods. The best linear fit of scatter plot exhibits moderate skill metrics: the slope is above 0.5 and

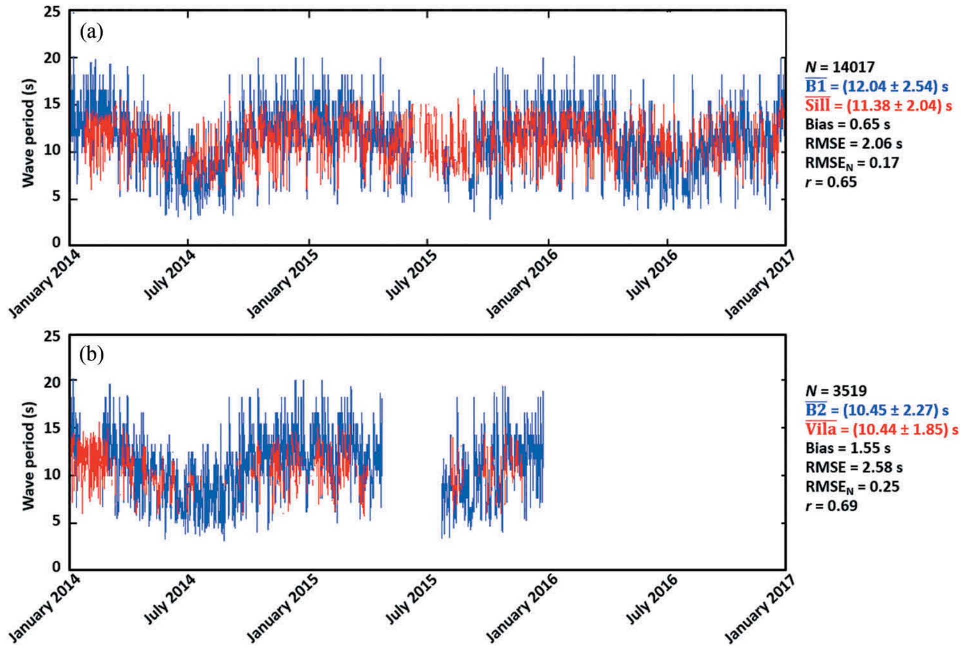

Figure 7. Validation of hourly wave period estimations provided by High-Frequency radar (red line) against in situ observations (blue line). (a) Sill site against B1 buoy, for the period 2014–2016. (b) Vila site against B2 buoy, for the period 2014–2015. Skill metrics are gathered on the right. N represents the number of hourly observations.

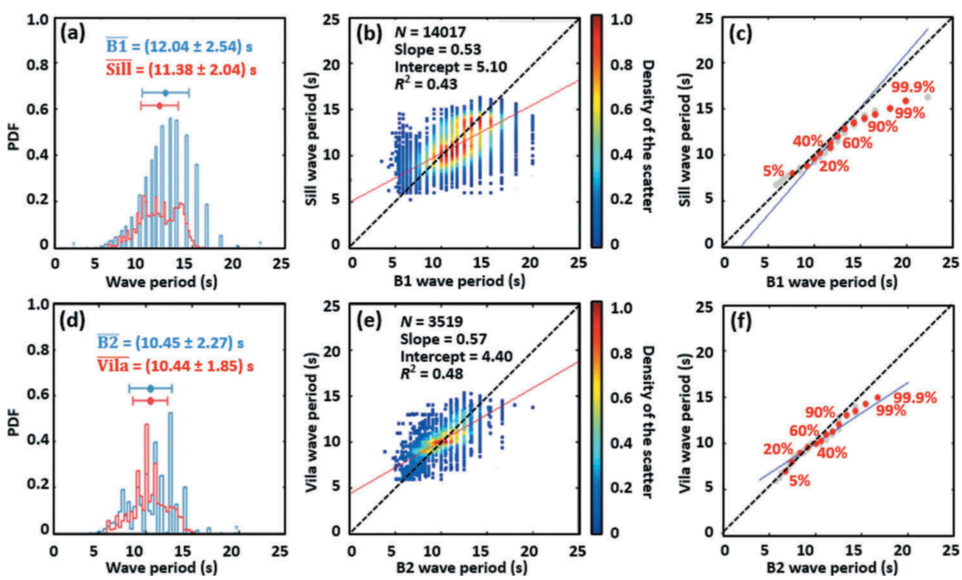

Figure 8. Histogram, best linear fit (red line) of scatter plot and QQ plot of wave period: (a-c) Sill radar site against B1 buoy, for the period 2014–2016. (d-f) Vila radar site against B2 buoy, for the period 2014–2015. In the QQ plot, 5–99.9% quantiles were established (red-filled dots). Dashed black lines represent the result of perfect agreement with slope 1.0 and intercept 0.

the associated R^2 (0.43), albeit significant, is lower than the obtained for H_s (Figure 8(b)). According to the QQ plot, there is a clear HFR underestimation of wave periods comprised between 80th and 100th percentiles but a consistent Sill performance for the rest of percentiles is evidenced (Figure 8(c)).

The 2-year comparison of Vila and B2 buoy wave period estimations reveals similar statistical distributions for both datasets, as reflected by the similar histograms and the corresponding metrics, with the mean wave period around 10.45 s (Figure 8(d)). The scatter presents lower dispersion and higher slope and R^2: 0.57 and 0.48, respectively (Figure 8(e)). Finally, the under prediction of the highest wave periods (above percentile 80) is not as marked for this radar site as the observed for Sill site (Figure 8(f)).

The Taylor diagrams of wave period illustrate that both Sill and Vila performances are rather alike, consistent and stable through different years, with r values emerging in the range 0.61–0.74 (Figure 9(a)). The quarterly analysis confirms that there are no significant disparities among seasons (Figure 9(b)), conversely to the results previously obtained for the significant wave height.

The seasonal features of the wave period in Galicia have been gathered in Table 4. Winter is characterized by the longest time-averaged wave periods, according to the in situ observations (above 13 s). HFR-derived centroid wave period estimations show both lower temporal variability and mean values, not only during wintertime (around 12 s) but also for autumn and spring. By contrast, a slight HFR overestimation is evidenced for summertime when the wave period precisely reaches its minimum value: mean values provided by Sill site and B1 buoy were 10.16 s and 10.09 s, respectively.

The most common wave conditions in Galicia have been characterized by determining the ranges of wave heights and periods that represent the majority of sea states (Figure 10). The scatter plots relating the significant wave height and period were computed for both in situ (B1 and B2 buoys) and remote-sensed estimations (Sill and Vila sites). Some similarities are observed between the scatter plots, despite the higher (lower) dispersion of HFR estimations for wave height (period). In addition, a linear

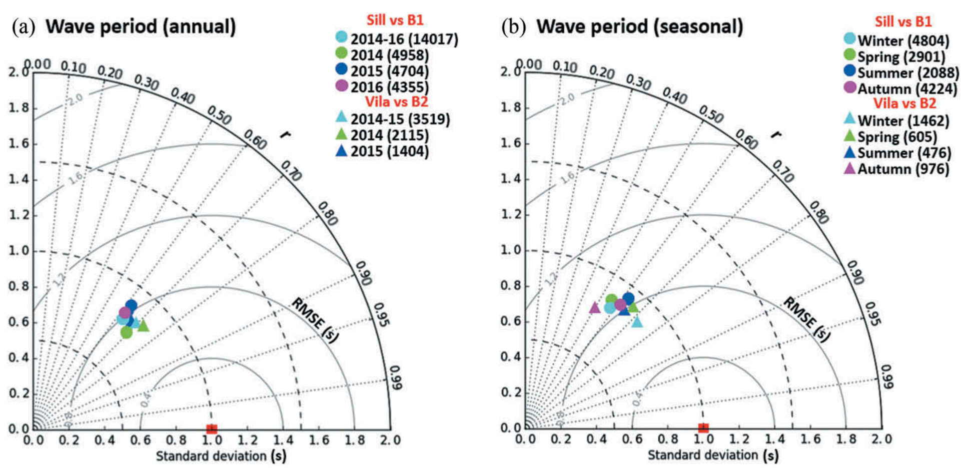

Figure 9. (a) Annual and (b) seasonal Taylor diagrams of wave period derived from the comparison of Sill (Vila) radar site against B1 (B2) buoy for the period 2014–2016 (2015–2016).

Table 4. Quarterly statistical metrics of wave period obtained for each instrument for the periods 2014–2016 (B1 and Sill) and 2014–2015 (B2 and Vila). *N* and SD represent the number of hourly observations and the standard deviation, respectively.

Season	Instrument	*N*	Mean (s)	SD (s)
Winter (J-F-M)	**B1 buoy**	4804	13.18	2.19
	Sill site	4804	12.07	1.82
	B2 buoy	1462	13.26	2.49
	Vila site	1462	11.34	1.82
Spring (A-M-J)	**B1 buoy**	2901	10.67	2.28
	Sill site	2901	10.67	1.94
	B2 buoy	605	10.78	2.39
	Vila site	605	9.26	1.59
Summer (J-A-S)	**B1 buoy**	2088	10.09	2.08
	Sill site	2088	10.16	1.91
	B2 buoy	476	9.31	2.21
	Vila site	476	9.57	1.56
Autumn (O-N-D)	**B1 buoy**	4224	12.63	2.29
	Sill site	4224	11.71	1.99
	B2 buoy	976	11.94	2.38
	Vila site	976	10.62	1.55

relationship between both parameters has been evidenced: extreme wave height events (above 9.4 m) also present the longest wave periods: 16–20 s and 13–16 s for buoys and HFR sites estimations, respectively. Conversely, low sea-states (below 3 m) are associated with the shortest wave periods (5–7 s). Based on the density distributions, it can be

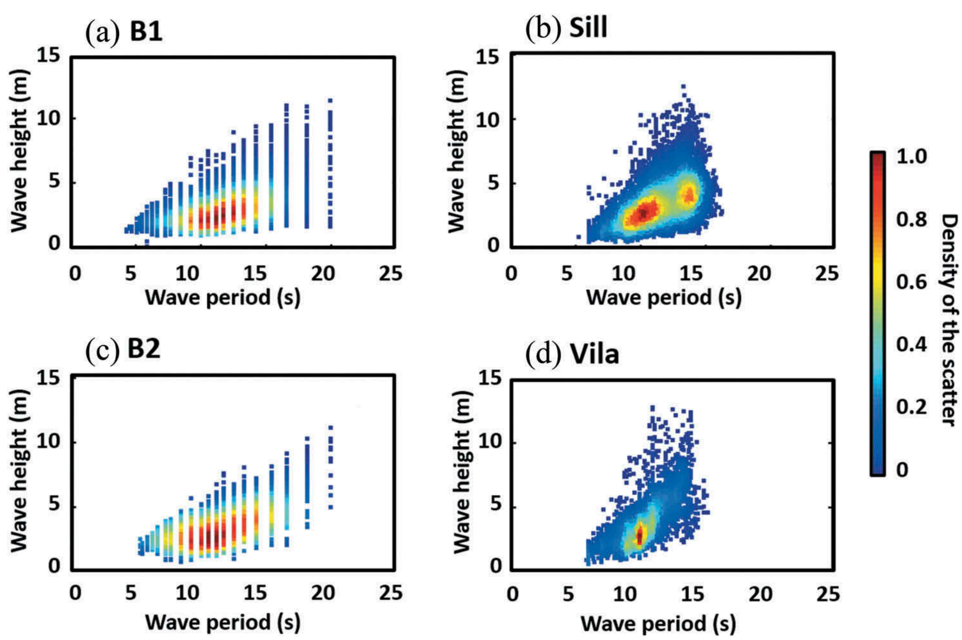

Figure 10. Scatter plots of significant wave height and wave period for a) B1 buoy and b) Sill radar site for a 3-year period (2014–2016); c) B2 buoy and d) Vila radar site for a two-year period (2014–2015). Centroid wave period and peak period data from radar sites and buoys, respectively, were used.

stated that the most usual wave events in the Galician coastal region are defined by wave heights and periods in the ranges 2–5 m and 8–15 s, respectively.

3.3. Mean wave direction

In terms of mean incoming wave direction, the concordance between B1 buoy and Sill radar site for the 3-year period analysed is noticeable, with NW and W-NW as the predominant sectors and residual waves coming from the NW-N and W-SW directions (Figure 11(a,b)). Such spatial distribution appears to be clearly influenced by the Galician coastline morphology and the periodic passage of cold fronts from the North Atlantic ocean. The seasonal analysis reveals that the most relevant wave height events ($H_s > 5$ m) usually take place during wintertime (Figure 11(c,d)) and to a lesser extent in autumn, with both instruments indicating a predominant north-westerly origin. By contrast, spring-like waves present a broader directional distribution and the three sectors from the second quadrant are almost equally prevalent (Figure 11(e,f)). During summer, the wave roses look rather alike: wave height events reach an annual minimum ($H_s < 3$ m) and, again, the prevailing incoming wave direction is the NW sector (Figure 11(g,h)). The global and seasonal skill metrics confirm the consistency of this HFR site performance, with r and RMSE values lying in the ranges 0.55–0.79 and 20° – 25°, respectively.

The main buoy-radar discrepancy lies in the underestimation (overestimation) of the number of wave events from the NW (W-NW) sector detected in remote-sensed observations. Such disagreement is even more pronounced for Vila site, as evidenced in Figure 12 (right column). A portion of the directional uncertainties can be attributed to wave propagation perpendicular to the direction of the HFR measurement. Previous researches indicated that substantial improvements in accuracy are feasible if two HFR sites are employed to survey the same patch of the ocean from two different directions (Toro et al. 2014; Gurgel, Essen, and Schlick 2006; Wyatt 1986.). Spurious contributions to the directional spectra (likely due to systematic radio interferences) might contaminate the radar backscatter signal and eventually lead to non-accurate mean wave direction estimations (Wyatt et al. 2003; López, Conley, and Greaves 2016). Such directional biases could be also enhanced in low sea states ($H_s < 2$ m) as a consequence of the aforementioned frequency limitations of a 5-MHz HFR system (section 3.1) and the subsequent collection of noisy estimations. This statement is supported by the lower-than-usual seasonal r values obtained in summer for Sill and Vila sites: 0.55 and 0.40, respectively.

Furthermore, a tendency for CODAR HFR-derived mean wave direction to be aligned more perpendicular to the coast compared to offshore in situ data has been previously reported (Kohut et al. 2008). Since the Galician coastline and the related depth contours present a north-south orientation (Figure 1(a)), such tendency might partially justify the recurrent HFR overestimation of wave events coming from the westernmost sector. Finally, the distance between the B1 buoy and the selected radar range cell is non-negligible (20 km). In this context, spatially variable wind directions and short-fetch conditions can play a role in the differences obtained.

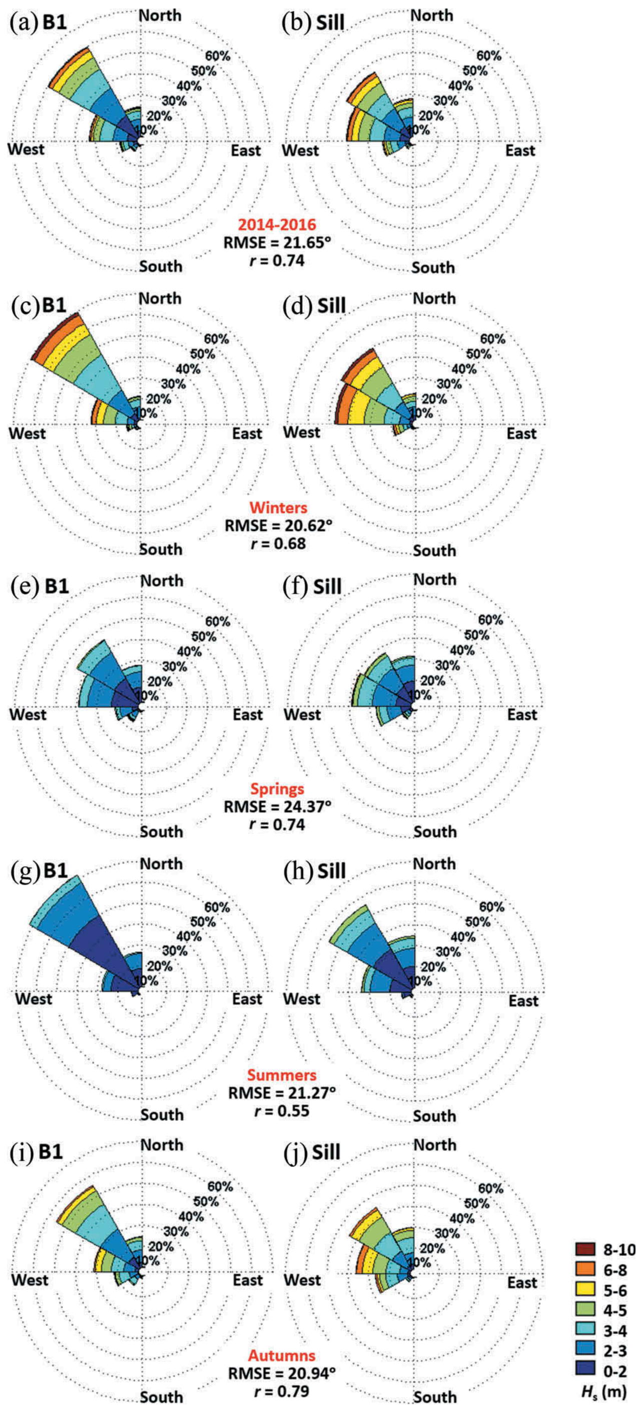

Figure 11. Comparison of the main incoming wave directions registered at B1 buoy (left) and Sill radar site (right) for a 3-year period (a-b) and on a seasonal basis (c-j).

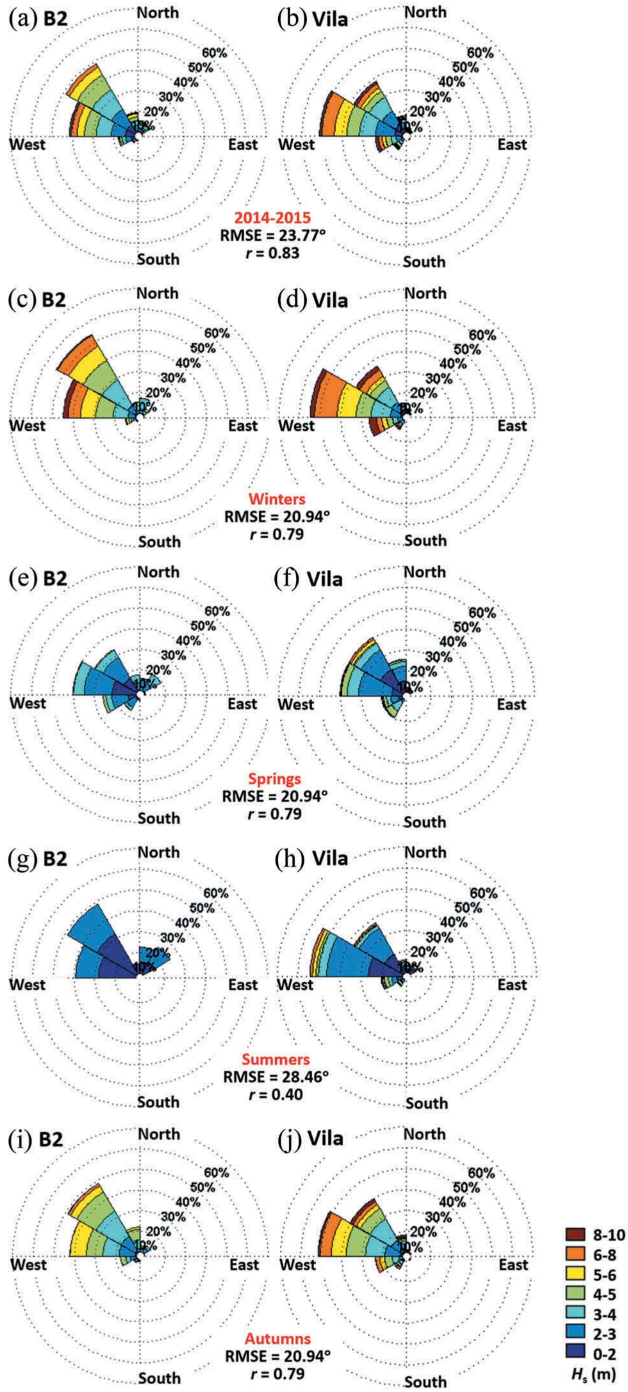

Figure 12. Comparison of the main incoming wave directions registered at B2 buoy (left) and Vila radar site (right) for a 2-year period (a-b) and on a seasonal basis (c-j).

3.4. NAO

The North Atlantic Oscillation (NAO) is a significant driver of climate variability in the Northern Hemisphere, particularly during the boreal winter months when the atmosphere is dynamically most active. Swings in the NAO index produce changes in the storms track and subsequently in the wind speed and direction over the Atlantic that alter the transport of heat and moisture. Previous studies have investigated the link between winter H_s variability in the Iberian Peninsula and the NAO index by means of wave buoy measurements and hindcast modelling (Semedo 2005; Almeida et al. 2011; Martínez-Asensio et al. 2016). When winter NAO is in its positive phase, storms usually track northeast of Europe and enhanced westerly winds induce higher than average waves in the northernmost Atlantic Ocean. Conversely, in the negative-NAO phase, the track of the storms is more zonal and south than usual due to a weakened Azores High. Thus, the trade winds, mid latitude westerlies, are slower and produce higher than average H_s in the Iberian Peninsula.

Such relationship has been qualitatively explored here by comparing the daily NAO index during both winter seasons (JFM) and the entire period (2014–2016) against remote-sensed wave estimations provided by Sill radar site (Figures 13 and 14, respectively). Vila site has not been used due to the aforementioned limited data availability. The scatter plots shown in Figure 13 reveal that winter NAO index is predominantly positive (90% of the time) during the analysed period 2014–2016. During the positive-NAO phase, there seems to be an overall tendency for higher wave height events, as reflected by the statistics (Figure 13(a)). Likewise, wave period values are higher during positive NAO (Figure 13(b)) since the storms, tracking towards the north of Europe, drive longer period swell from the northwest (mean incoming angle of 303º, clockwise from true north). By contrast, negative-NAO storms have associated shorter period swell arriving to Galicia from a more westerly direction, with a mean incoming angle around 278º, as indicated in Figure 13(c).

The daily evolution of both NAO index and anomalies of peak wave height (relative to the mean value) estimated at Sill radar site during the 3-year study period are exhibited

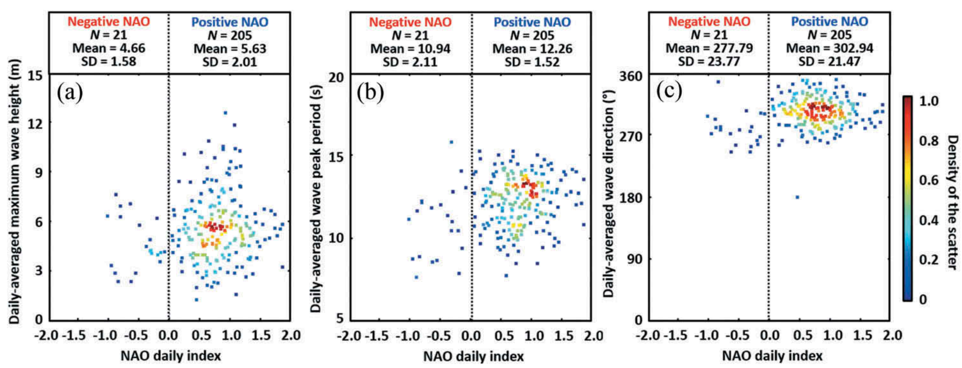

Figure 13. Scatter plots of a) significant wave height, b) centroid wave period and c) mean wave direction provided by Sill radar site, as a function of the winter (JFM) North Atlantic Oscillation (NAO) daily index, for the 3-year period 2014–2016. Statistical metrics for negative and positive phases of NAO are gathered on top boxes. N and SD represent the number of daily values and the standard deviation, respectively.

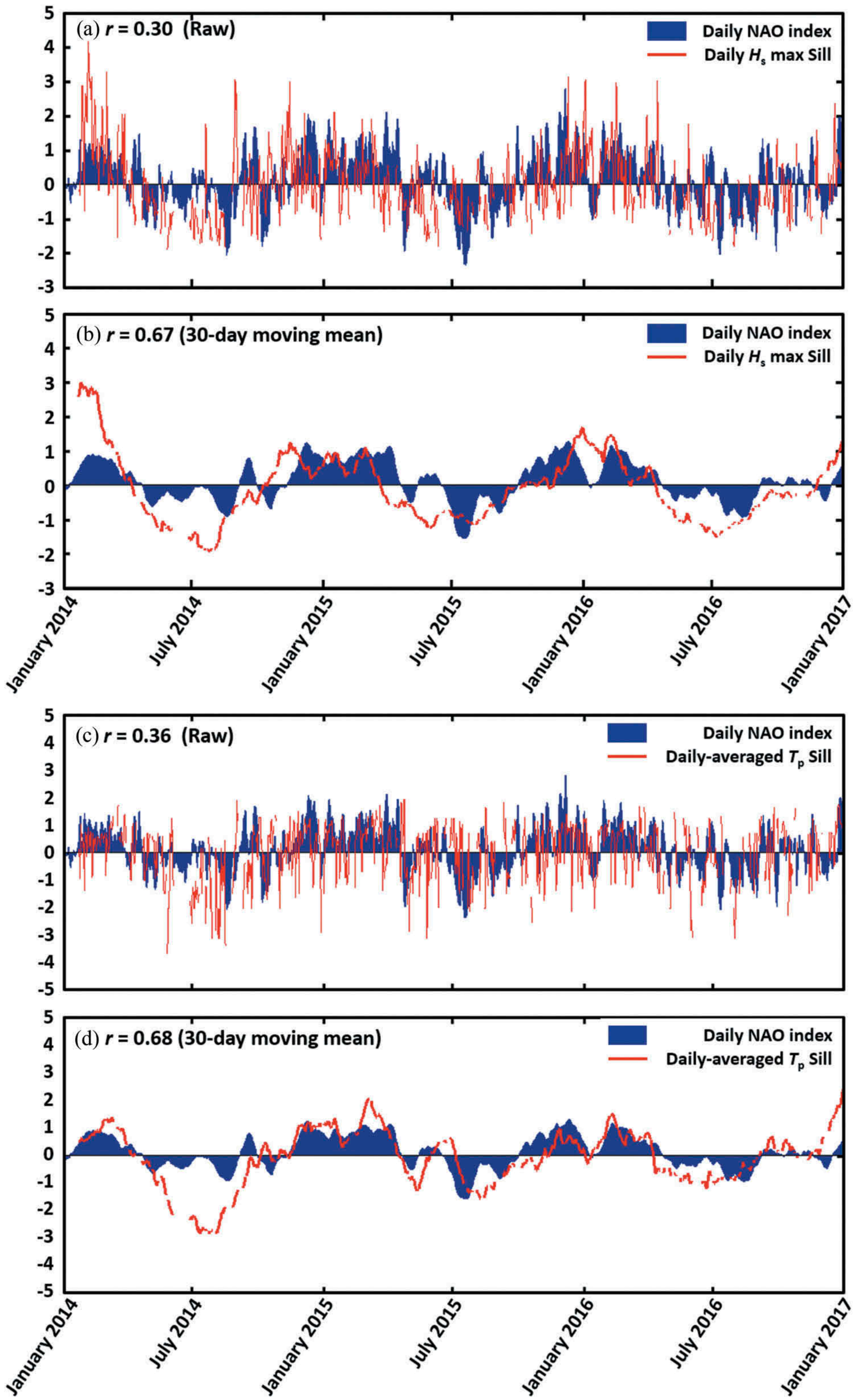

Figure 14. Daily evolution of the North Atlantic Oscillation (NAO) index (blue bars) and anomalies of peak wave height estimated by Sill radar site (H_s, red line) during a 3-year period (2014–2016) for raw (a) and a 30-day moving mean (b) time series. Daily evolution of NAO index (blue bars) and anomalies of centroid wave period (T_p, red line) estimated by Sill for raw (c) and a 30-day moving mean (d) time series.

in Figure 14(a). There seems to be a direct relationship between the two variables with strongly positive winter NAO indices corresponding to higher than average H_s estimations and vice versa, strongly negative-NAO indices corresponding to lower than average H_s radar measurements in the Galician coast. The positive r value, albeit moderate (0.30), is still statistically significant. After applying a 30-day moving average to smooth out the natural data scatter, such relationship becomes stronger at monthly timescale and the correlation increases up to 0.67 (Figure 14(b)). This finding is not in complete agreement with similar researches previously focused on the Iberian Peninsula. Semedo (2005) and Almeida et al. (2011) reported a negative correlation between the winter NAO index and the significant wave height recorded by in situ devices in Portugal. Martínez-Asensio et al. (2016) computed winter (DJFM) regression coefficient between NAO index and hindcasted H_s anomalies for the period 1989–2009, showing a moderate and positive correlation for the northern coast of the Iberian Peninsula but an inverse relationship for the entire Galician and Portuguese coast. Since the northern Galician coast appeared in this work as the transition zone where the r value swung from positive to negative, it seems reasonable to hypothesize, based on the results here presented, that such shift in NAO influence could take place at slight lower latitudes, close to the Portugal–Galicia border (41ºN, Figure 1). Notwithstanding, additional efforts should be devoted to shed light on this issue.

The evolution of the daily averaged HFR-derived wave centroid period appears to be also linked to the NAO index, as stated by a positive r value of 0.36 (Figure 14(c)). Smoothed time series, obtained after imposing a 30-day moving mean, present a relevant connection as reflected by an r value of 0.68 (Figure 14(d)). This finding is in close agreement with results previously reported by Martínez-Asensio et al. (2016), where the MWP was found to be positively correlated with the winter (DJFM) NAO index in the area between the North Sea, the Bay of Biscay and the west coast of the Iberian Peninsula.

Notwithstanding, a significant interdependence could not be found between the daily NAO index and the daily averaged incoming wave direction provided by Sill site (not shown). Such lack of correlation might be attributed to the aforementioned directional biases (likely due to noisy contributions to the directional spectra) or the already reported overall tendency for CODAR HFR-derived mean wave direction to be aligned more perpendicular to the coast.

Therefore, the NAO has a major impact on the northernmost latitudes of Europe but limited influence on the inter-annual variations of H_s in the Galician coast where other modes of interannual atmospheric variability, such as the East Atlantic (EA), may also play a relevant role (Martínez-Asensio et al. 2016). Whereas the NAO index is able to explain only a small percentage of the variation in wave height, more local factors could be of importance in controlling storminess in the west coast of the Iberian Peninsula (Almeida et al. 2011). In this context, there are nowadays valuable efforts to define novel climate indexes to better explain winter wave height variability along the coast of south-western Europe, such as the Western Europe Pressure Anomaly (WEPA; Castelle et al. 2017). The WEPA index is based on the sea level pressure gradient between the station Valentia (Ireland) and Santa Cruz de Tenerife (Canary Islands). Future works of this nature should address the connection between HFR-derived wave height estimations and WEPA index and how such the latter modulates the former.

Since HFR performance is more accurate for high sea-states (Figure 6(b)) and the subtle but real connection between the NAO and HFR wave estimations in Galicia (Figures 13 and 14) has been shown, it is worth attempting to elucidate whether the skill of the HFR system fluctuates depending on the NAO phase. In terms of significant wave height, strongly positive-NAO indices correspond to higher than average H_s estimations and vice versa. Therefore, we could a priori expect a higher skill for this type of situation rather than for negative-NAO phase events, which have associated – on average – calmer sea conditions. However, such a hypothesis is not supported by the $RMSE_N$ values shown in Figure 15, as no substantial differences in HFR accuracy could be found between positive and negative-NAO cases for each of the three wave parameters. Only slight discrepancies are observed in *r* and RMSE values, probably due to the fact that positive-NAO events include the most extreme H_s (above 9.4 m) but also relatively calm H_s (below 3 m) episodes (Figure 15(a)). In the same vein, statistical metrics derived from the comparison of centroid wave period do not allow us to postulate that HFR

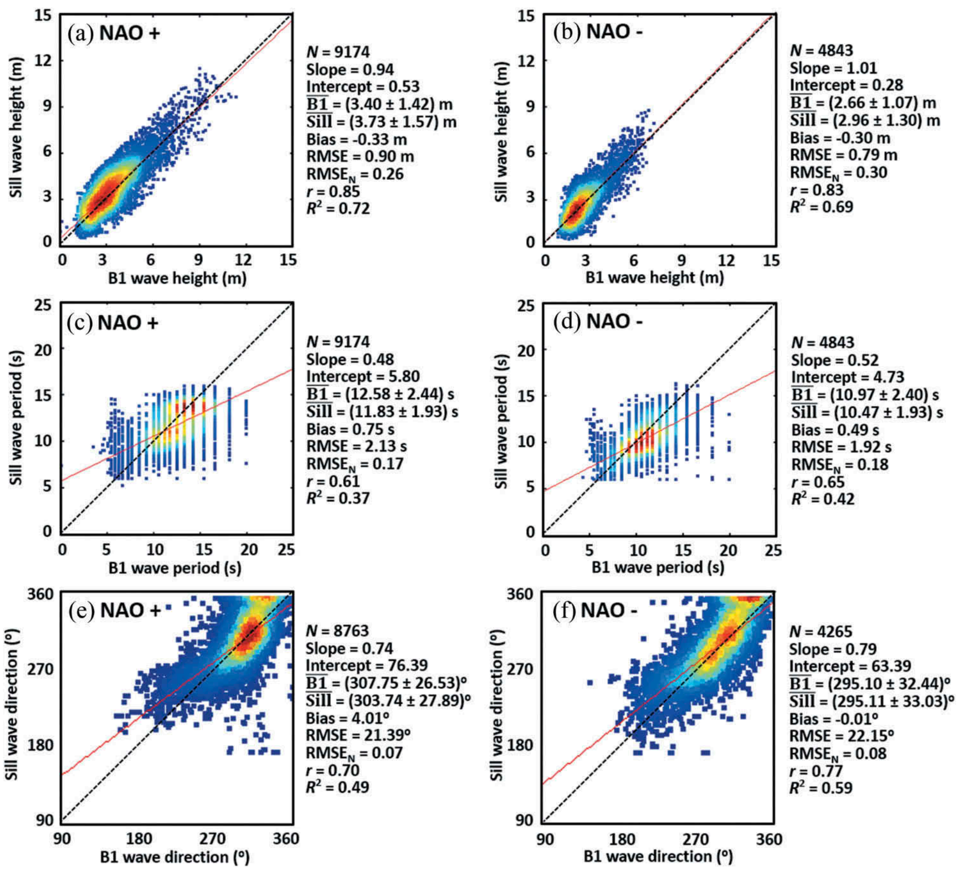

Figure 15. Best linear fit (red line) of scatter plot between B1 buoy and Sill radar-derived hourly estimations of significant wave height (a-b), wave period (c-d) and mean wave direction (e-f), for positive-NAO phase (left column) and negative-NAO phase (right column), during the period 2014–2016. Dashed black lines represent the result of perfect agreement with slope 1.0 and intercept 0. Skill metrics are gathered on the right.

accuracy is NAO-phase dependent, despite the fact that r (RMSE) value is slightly higher (lower) for negative-NAO indices (Figure 15(c,d)). In terms of mean wave direction, higher r is obtained for negative (0.77) than for positive (0.70) NAO events (Figure 15 (e,f)). This could be attributable to both the aforementioned directional bias in HFR estimations (where wave events from the westernmost sector are overestimated) and the predominant westerly direction of negative-NAO storms. In summary, no evidences have been found of a significant link between fluctuations in HFR performance and swings in NAO index.

4. Conclusions

Since the validity of HFR-derived wave estimations is still under scrutiny, a long-term multi-parameter skill assessment of a 5-MHz CODAR SeaSonde HFR network deployed along the Galician Coast was attempted for 2014–2016 in order to quantify the uncertainties related to this technology. To this aim, wave estimations from two radar sites obtained directly by the CODAR radar proprietary software, were independently validated against quality-controlled in situ hourly observations from two moored buoys for two different periods.

The accuracy assessment of CODAR HFR-derived significant wave height revealed a consistent agreement, with r values above 0.75 and normalized root mean squared error ($RMSE_N$) below 0.4, in accordance with previous results reported in the literature (Table 1). Despite the restricted data availability, the precision of Vila site measurements was also consistent, albeit not so high. The analysis on a quarterly basis demonstrated that HFR performance was more accurate in winter and autumn when severe wave height events (above percentile 90th) usually take place, with H_s usually exceeding 6 m. By contrast, the precision and availability of CODAR HFR-derived estimations during summertime (calmer sea states) seem to be lower because the second-order spectrum is closer to the noise floor and more likely to be contaminated with systematic interferences that result in a well-documented wave height overestimation and a limited temporal continuity in wave measurements (Lipa et al. 2018).

A plausible cause for the detected overestimation in H_s measurements could lie in the assumptions made in the inversion method. The Pierson-Moskowitz fit-to-spectrum unimodal model used here has previously proved its validity to properly describe wind-dominated seas and also swell dominated seas, whereas this might be different under some combination of multi-modal sea-states under complex met-ocean conditions (Lipa et al. 2018). An additional factor that might contribute to the discrepancies observed in H_s in this tidally dominated region consists of the hydrodynamic modulations of waves by periodic underlying currents, previously reported to be more intense in HFR estimations (Barrick and Lipa 2015). Further investigation on waves–current interaction should be undertaken in the future.

In the case of the centroid wave period, Sill and Vila performances were similar, consistent and stable through different years, with r values emerging in the range 0.61–0.74. The quarterly analysis confirmed that there were not significant discrepancies among seasons. In terms of mean incoming wave direction, the directional accuracy was moderately good, with NW and W-NW as the predominant sectors and r values ranging from 0.55 to 0.79. The main buoy-radar discrepancy lied in the underestimation (overestimation) of the number of wave events from the NW (W-NW) sector detected in the remote-sensed observations. A portion of the observed directional uncertainties might be attributed to: i) the fact that HFR systems can only detect wave propagation in the radial direction, moving away or towards the radar site; ii) occasional radio interferences, ship echoes or intense current variability that can be interpreted as noisy contributions to the directional spectrum (Wyatt, Thompson, and Burton 1999); iii) a tendency for CODAR HFR-derived mean wave direction to be aligned more perpendicular to the coast compared to offshore in situ data has been previously reported (Kohut et al. 2008). Since the Galician coastline presents a north-south orientation, such a tendency might partially justify the permanent overestimation of wave events coming from the westernmost sector.

Despite the discrepancies mentioned, in situ buoys and HFR measurements appear to capture similar wave features and temporal variability. Therefore, it seems reasonable to assume that a portion of the differences could be inherently attributed to the different sampling techniques. Whereas CODAR HFR systems provide wave data averaged over range rings (assuming homogeneity over the whole of each circular range cell), buoys give point measurements. In this context, coastal effects can also lead to locally varying wave fields and make absolute comparisons between in situ and remote-sensing instruments even harder.

Nevertheless, and according to these results, it can be concluded that properly treated CODAR radar-derived wave estimations can be potentially employed for operational coastal monitoring across a wide range of sea states. The HFR system operates within tolerance ranges and observed error levels are in line with those values previously published. Additional development efforts should focus on the implementation of a more refined quality-control protocol and fine-tuning in order to have the right trade-off between confirmed outlier identification and false alarm rate (Cosoli et al. 2018; Hisaki 2009). Dedicated emphasis should be placed on filtering spike-like fluctuations, especially for Vila site as there is still room for improvement. Given the heterogeneity of the Galician coast, each radar coverage area has unique characteristics in terms of coastline morphology, bathymetry and subsequent coastal effects such as wave refraction, damping and breaking (Wyatt et al. 2005). Therefore, site-specific-tailored quality-control methodologies based on the particular local environment are required to ensure robust radar measurements. Ongoing actions cover the implementation and validation of a new Doppler cross-spectra processing along with new and updated configurations for Vila radar site (Basañez et al. 2018). Such an approach increases the number of range cells considered and aims to minimize the contribution of unrealistic features by better discriminating between reliable estimations and spurious values.

The vulnerability of the parameter estimates to the aforementioned low-frequency noise, and the subsequent gappy nature of radar-derived datasets could be reduced by using a multi-frequency HFR system. By switching transmit frequency from 5 to 13 MHz during low and moderate sea states (mainly concentrated during summer and spring times), the measuring performance of widely changing H_s could be significantly enhanced. The combined estimation based on results of both frequencies would solve the wave height limitation at a single frequency and also reduce radio interferences in low waves (Wyatt and Green 2009; Tian, Wen, and Zhou 2014).

As the wintertime variability of the North Atlantic cyclonic activity is primarily modulated by the North Atlantic Oscillation (NAO), its influence on the inter-annual variations of HFR-derived daily averaged wave data has been investigated in the Galician coast for both winter seasons (JFM) and the entire period (2014–2016). Results revealed the moderate (but statistically significant) positive correlation between the daily NAO index and Sill site estimations of significant wave height and centroid wave period. There seems to be a direct relationship between the two variables with strongly positive-NAO indices corresponding to higher than average H_s and period estimations and vice versa. However, since NAO index appears to explain only a small percentage of the variation in wave height, other modes of atmospheric variability and additional local factors may be of importance in controlling storminess in the west coast of the Iberian Peninsula (Almeida et al. 2011). Finally, the HFR system skill was evaluated under positive and negative-NAO conditions in order to elucidate whether the radar accuracy is or is not NAO-phase dependent. No substantial differences could be found for each of the three parameters analysed as HFR accuracy remained mostly unaffected by swings in the NAO index.

Future research lines might include the use in the concert of in situ and HFR wave records as a consistent benchmark to quantitatively validate the outputs from operational wave forecasting systems (Lorente et al. 2018). Likewise, HFR derived wave parameters could be employed in tandem with modelling tools in order to assess both the potential of the Galician coast for energy production and the optimum locations for wave farms (Iglesias et al. 2009; Proença, Conley, and Greaves 2012; Atan, Goggins, and Nash 2016b). The resource characterization is particularly crucial as the wave climate in Galicia is among the harshest in Europe, with an estimated annual wave energy clearly above 250 MWh m^{-1}. Finally, assimilation of HFR-derived wave parameters remains as a future work line to enhance model predictive skills and properly portray the main features of the wave field in the Galician region.

Acknowledgements

The authors gratefully acknowledge (i) Qualitas Remos Company for their useful technical suggestions; (ii) INTECMAR - Consellería do Mar - Xunta de Galicia for providing the HF radar wave data (Vila site) and iii) NOAA, for the NAO climate indices. This work has been carried out within the frame of MyCOAST project.

Funding

This work was supported by the INTERREG Atlantic Area Project MyCOAST (EAPA 285/2016) co-funded by the ERDF (EU).

References

Alfonso, M., E. Álvarez-Fanjul, and J. D. López. 2006. “Comparison of CODAR SeaSonde HF Radar Operational Waves and Currents Measurements with Puertos Del Estado Buoys”. *Final internal report of Puertos del Estado*: 1–32.

Almeida, I. P., O. Ferreira, M. I. Vousdoukas, and G. Dodet. 2011. "Historical Variation and Trends in Storminess along the Portuguese South Coast." *Natural Hazards and Earth System Sciences* 11: 2407–2417. doi:10.5194/nhess-11-2407-2011.

Atan, R., J. Goggins, M. Hartnett, P. Agostinho, and S. Nash. 2016a. "Assessment of Wave Characteristics and Resource Variability at a ¼-Scale Wave Energy Test Site in Galwat Bay Using Waverider and High Frequency Radar (CODAR) Data." *Ocean Engineering* 117: 272–291. doi:10.1016/j.oceaneng.2016.03.051.

Atan, R., J. Goggins, M. Hartnett, S. Nash, and P. Agostinho. 2015. "Assessment of Extreme Wave Height Events in Galway Bay Using High Frequency Radar (CODAR) Data." *Renewable Energies Offshore* 49–56. doi:10.1201/b18973-8.

Atan, R., J. Goggins, and S. Nash. 2016b. "A Detailed Assessment of the Wave Energy Resource at the Atlantic Marine Energy Test Site." *Energies* 9 (11): 967. doi:10.3390/en9110967.

Barrick, D. E. 1977. "Extraction of Wave Parameters Form Measured HF Radar Sea Echoes Spectra." *Radio Science* 12 (3): 415–424. doi:10.1029/RS012i003p00415.

Barrick, D. E., and B. Lipa. 2015. "When are HF-radar Observed Wave Heights Modulated by Periodic Tidal and Inertial Currents?" *Paper presented at Current, Waves and Turbulence Measurement, MTS-IEEE*, Florida, 2–6 March. doi: 10.1109/CWTM.2015.7098142.

Barrick, D. E., M. W. Evans, and B. L. Weber. 1977. "Ocean Surface Currents Mapped by Radar." *Science* 198: 138–144. doi:10.1126/science.198.4313.138.

Basañez, A., B. Vila, P. Montero, P. Lorente, E. Álvarez-Fanjul, and V. Pérez-Muñuzuri. 2018. "Steps to Improve the Wave Data Estimated by HF Radars". *Poster presented at Physical Oceanography Meeting, EOF*, Vigo, Spain, 20–22 June.

Castelle, B., G. Dodet, G. Masselink, and T. Scott. 2017. "A New Climate Index Controlling Wave Activity along the Atlantic Coast of Europe: The West Europe Pressure Anomaly." *Geophysical Research Letters* 44. doi:10.1002/2016GLO72379.

Chen, Z., C. Zezong, J. Yanni, F. Lingang, and Z. Gengfei. 2013. "Exploration and Validation of Wave-Height Measurement Using Multifrequency HF Radar." *Journal of Atmospheric and Oceanic Technology* 30: 2189–2202. doi:10.1175/JTECH-D-12-00178.1.

Copernicus Marine In situ Team. 2017. *Copernicus in Situ TAC, Real Time Quality Control for WAVES*. Toulouse, France: Copernicus in situ TAC, 1–19. doi:10.13155/46607.

Cosoli, S., B. Grcic, S. De Vos, and Y. Hetzel. 2018. "Improving Data Quality for the Australian High Frequency Ocean Radar Network through Real-Time and Delayed-Mode Quality-Control Procedures." *Remote Sensing* 10: 1476. doi:10.3390/rs10091476.

Crombie, D. D. 1955. "Doppler Spectrum of Sea Echo at 13.56 Mc/S." *Nature* 175: 681–682. doi:10.1038/175681a0.

Emery, W. J., and R. E. Thompson. 2001. *Data Analysis Methods in Physical Oceanography*. ISBN 9780080477008. Amsterdam: Elsevier Science. 654.

Fernandez, D. M., H. C. Graber, J. D. Paduan, and D. E. Barrick. 1997. "Mapping Wind Direction with HF Radar." *Oceanography* 10 (2): 93–95. doi:10.5670/oceanog.1997.33.

Forney, R., H. Roarty, and S. Glenn. 2015. "Measuring Waves with a Compact HF Radar". *Paper presented at OCEANS 2015 - MTS/IEEE*, Washington, 19–22 October.

Gómez, R., T. Helzel, L. Wyatt, G. Lopez, D. Conley, N. Thomas, S. Smet, and G. Sicot. 2015. "Estimation of Wave Parameters from HF Radar Using Different Methodologies and Compared with Wave Buoy Measurements at the Wave Hub". *Paper presented at OCEANS 2015 - MTS/IEEE*, Genova, 18–21 May.

Graber, H. C., and M. L. Heron. 1997. "Wave Height Measurement from HF Radar." *Oceanogr* 10: 90–92. doi:10.5670/oceanog.1997.32.

Gurgel, K. W., G. Antonischski, H. H. Essen, and T. Schlick. 1999. "Wellen Radar (WERA): A New Ground Wave Radar for Remote Sensing." *Coastal Engineering* 37: 219–234. doi:10.1016/S0378-3839(99)00027-7.

Gurgel, K.-W., -H.-H. Essen, and T. Schlick. 2006. "An Empirical Method to Derive Ocean Waves from Second-Order Bragg Scattering: Prospects and Limitations." *IEEE Journal of Oceanic Engineering* 31: 804–811. doi:10.1109/JOE.2006.886225.

Hisaki, Y. 2006. “Ocean Wave Directional Spectra Estimation from an HF Ocean Radar with a Single Antenna Array: Methodology.” *Journal of Atmospheric and Oceanic Technology* 23 (2): 268–286. doi:10.1175/JTECH1836.1.

Hisaki, Y. 2009. “Quality Control of Surface Wave Data Estimated from Low Signal-to-Noise Ratio HF Radar Doppler-Spectra.” *Journal of Atmospheric and Oceanic Technology* 26: 2444–2461. doi:10.1175/2009JTECHO653.1.

Hurrel, J. W. 1995. “Decadal Trends in the North Atlantic Oscillation: Regional Temperatures and Precipitation.” *Science* 269 (5224): 676–679. doi:10.1126/scince.269.5224.676.

Iglesias, G., M. López, R. Carballo, A. Castro, J. A. Fraguela, and P. Frigaard. 2009. “Wave Energy Potential in Galicia (NW Spain).” *Renawable Energy* 34: 2323–2333. doi:10.1016/j.renene.2009.03.030.

James, C., M. Collopy, L. R. Wyatt, and A. Middleditch. 2019. “Suitability of the Southern Australia Integrated Marine Observing System´S (SA-IMOS) HF-Radar for Operational Forecasting”. *Journal of Operational Oceanography*. doi:10.1080/1755876X.2019.1567450.

Kohut, J., H. Roarty, S. Licthenwalner, S. Glenn, D. Barrick, B. Lipa, and A. Allen. 2008. “Surface Currents and Wave Validation of a Nested Regional HF Radar Network in the Mid-Atlantic Bight”. Paper presented at IEEE/OES/CMTC 9th Working Conference on Current Measurement Technology, March 17–19, Charleston, SC.

Lipa, B. J., M. Daugharty, M. Fernandes, D. Barrick, A. Alonso-Martirena, H. Roarty, J. Dicopoulos, and C. Whelan. 2018. “Developments in Compact HF Radar Ocean Wave Measurements.” In *Physical Sensors, Sensor Networks and Remote Sensing. Book Series: Advances in Sensors: Reviews,* Vol. 5, edited by S. Yurish, 469–495. Barcelona, Spain: International Frequency Sensor Association Publishing (IFSA).

Lipa, B. J., and B. Nyden. 2005. “Directional Wave Information from the SeaSonde.” *IEEE Jounal of Oceanic Engineering* 30 (1): 221–231. doi:10.1109/JOE.2004.839929.

Lipa, B. J., B. Nyden, D. Barrick, and J. Kohut. 2008. “HF Radar Sea-Echo from Shallow Water.” *Sensors* 8: 4611–4635. doi:10.3390/s8084611.

Lipa, B. J., D. Barrick, A. Alonso-Martirena, M. Fernandes, M. Ferrer, and B. Nyden. 2014. “Brahan Project High Frequency Radar Ocean Measurements: Currents, Winds, Waves and Their Interactions.” *Remote Sensing* 6 (12): 12094–12117. doi:10.3390/rs61212094.

Long, R. M., D. Barrick, J. L. Largier, and N. Garfield. 2011. “Wave Observations from Central California: SeaSonde Systems and in Situ Wave Measurements.” *Journal of Sensors* 2011: 1–18. doi:10.1155/2011/728936.

López, G., D. Conley, and D. Greaves. 2016. “Calibration, Validation and Analysis if an Empirical Algorithm for the Retrival of Wave Spectra from HF Radar Sea Echo.” *Journal of Atmospheric and Oceanic Technology* 33: 245–261. doi:10.1175/JTECH-D-15-0159.1.

Lorente, P., M. G. Sotillo, L. Aouf, A. Amo-Baladrón, E. Barrera, A. Dalphinet, C. Toledano et al. 2017. “The New CMEMS IBI-WAV Forecasting System: Skill Assessment Using in Situ and HF Radar.” *8th EuroGOOS Conference*, Bergen, 2–5 October.

Lorente, P., M. G. Sotillo, L. Aouf, A. Amo-Baladrón, E. Barrera, A. Dalphinet, C. Toledano, et al. 2018. ““Extreme Wave Height Events in NW Spain: A Combined Multi-Sensor and Model Approach“.” *Remote Sensing* 10 :1. doi:10.3390/rs10010001.

Lorente, P., S. Piedracoba, and E. Álvarez-Fanjul. 2015. “Validation of High-Frequency Radar Ocean Surface Current Observations in the NW of the Iberian Peninsula.” *Continental Shelf Research* 92: 1–15. doi:10.1016/j.csr.2014.11.001.

Lorente, P., S. Piedracoba, J. Soto-Navarro, M. I. Ruiz, E. Álvarez-Fanjul, and P. Montero. 2016. ““The High Frequency Coastal Radar Network Operated by Puertos Del Estado (Spain): Roadmap to a Fully Operational Implementation“.” *IEEE Journal of Oceanic Engineering* 42 (1): 56–72. doi:10.1109/JOE.2016.2539438.

Martínez-Asensio, A., M. N. Tsimplis, M. Marcos, X. Feng, D. Gomis, G. Jordá, and S. A. Josey. 2016. ““Response of the North Atlantic Wave Climate to Atmospheric Modes of Variability“.” *International Journal of Climatology* 36: 1210–1225. doi:10.1002/joc.4415.

Orasi, A., M. Picone, A. Drago, F. Capodici, A. Gauci, G. Nardone, R. Inghilesi, et al. 2018. ““HF Radar for Wind Waves Measurements in the Malta-Sicily Channel“.” *Measurements* 128: 446–454.

Prandle, D. 1991. “A New View of Near-Shore Dynamics Based on Observations from HF Radar.” *Progress in Oceanography* 27: 403–438. doi:10.1016/0079-6611(91)90030-P.

Proença, B., D. Conley, and D. Greaves. 2012. “Initial Evaluation of a WERA HF Radar as a Resource Assessment Tool for Wave Energy.” *Paper presented at the International Conference on Ocean energy (ICOE)*, Dublin, 17–19 October. doi: 10.1094/PDIS-11-11-0999-PDN

Quentin, C., B. Zakardjian, L. Marié, A. Rubio, A.-C. Bennis, F. Dumas, A. Sentchev, et al. 2017. ““Progress Towards a French High Frequency Ocean Surface Wave Radar Network“.” *Mercator Ocean Journal* 55: 25–38.

Ramos, R. J., H. C. Graber, and B. K. Haus. 2009. ““Observation of Wave Energy Evolution in Coastal Areas Using HF Radar“.” *Journal of Atmospheric and Oceanic Technology* 26: 1891–1909. doi:10.1175/2009JTECHO631.1.

Rubio, A., J. Mader, L. Corgnati, C. Mantovani, A. Griffa, A. Novellino, C. Quentin, et al. 2017. ““HF Radar Activity in European Coastal Seas: Next Steps Towards a Pan-European HF Radar Network“.” *Frontiers in Marine Science* 20. doi:10.3389/fmars.2017.00008.

Saviano, S., A. Kalampokis, E. Zambianchi, and M. Uttieri. 2019. “A Year-Long Assessment of Wave Measurements Retrieved from an HF Radar Network in the Gulf of Naples (Tyrrhenian Sea, Western Mediterranean Sea).” *Journal of Operational Oceanography* 12: 1–15. doi:10.1080/1755876X.2019.1565853.

Saviano, S., G. A. Besio, M. Uttieri, and E. Zambianchi. 2017. “Wave Measurement and Models in the Tyrrhenian Sea.” *Poster presented at the European Geosciences Union*, *Vol. 19, EGU2017-1569*, Vienna, 23–28 April.

Schmidt, R. 1986. ““Multiple Emitter Location and Signal Parameter Estimation“.” *IEEE Transactions on Antennas and Propagation* 34: 276–280. doi:10.1109/TAP.1986.1143830.

Semedo, A. 2005. “The North Atlantic Oscillation Influence on the Wave Regime in Portugal: An Extreme Wave Event Analysis.” *Master of Science in Physical Oceanography, Naval Postgraduate School*.

Shearman, E. D. R., and M. D. Moorhead. 1988. “Pisces: A Coastal Ground-Wave Radar for Current, Wind and Wave Mapping to 200 Km Ranges.” *In International Geoscience and Remote Sensing Symposium,'remote Sensing: Moving toward the 21st Century* 2 773–776.IEEE

Siddons, L. A., L. R. Wyatt, and J. Wolf. 2009. “Assimilation of HF Radar Data into the SWAN Wave Model.” *Journal of Marine Systems* 77 (3): 312–324. doi:10.1016/j.jmarsys.2007.12.017.

Taylor, K. E. 2001. ““Summarizing Multiple Aspects of Model Performance in a Single Diagram“.” *Journal of Geophysical Research* 106: 7183–7192. doi:10.1029/2000JD900719.

Tian, Y., B. Wen, and H. Zhou. 2014. ““Measurement of High and Low Waves Using Dual-Frequency Broad-Beam HF Radar“.” *IEEE Geoscience and Remote Sensing Letters* 11 (9): 1599–1603. doi:10.1109/LGRS.2014.2301837.

Tian, Y., B. Wen, H. Zhou, C. Wang, J. Yang, and W. Huang. 2017. “wave Height Estimation from First-Order Backscatter of a Dual-Frequency High Frequency Radar.” *Remote Sensing* 9: 1186. doi:10.3390/rs9111186.

Toro, V. G., F. J. Ocampo-Torres, P. Osuna, H. García-Nava, X. Flores-Vidal, and R. Durazo. 2014. “Analysis of Fetch-Limited Wave Growth Using High-Frequency Radars in the Gulf of Tehuantepec.” *Ciencias Marinas* 40 (2): 113–132. doi:10.7773/cm.v40i2.2403.

Waters, J., L. R. Wyatt, J. Wolf, and A. Hines. 2013. “Data Assimilation of Partitioned HF Radar Wave Data into Wavewatch III.” *Ocean Modelling* 72: 17–31. doi:10.1016/j.ocemod.2013.07.003.

Wyatt, L. R. 1986. “The Measurement of the Ocean Wave Directional Spectrum from HF Radar Doppler Spectra.” *Radio Science* 21: 473–485. doi:10.1029/RS021i003p00473.

Wyatt, L. R. 1990. “A Relaxation Method for Integral Inversion Applied to HF Radar Measurement of the Ocean Wave Directional Spectrum.” *International Journal of Remote Sensing* 11 (8): 1481–1494. doi:10.1080/01431169008955106.

Wyatt, L. R. 2018. “A Comparison of Scatterometer and HF Radar Wind Direction Measurements.” *Journal of Operational Oceanography* 11: 54–63. doi:10.1080/1755876X.2018.1443625.

Wyatt, L. R., G. Liakhovetski, H. C. Graber, and B. K. Haus. 2005. “Factors Affecting the Accuracy of SHOWEX HD Radar Wave Measurements.” *Journal of Atmospheric and Oceanic Technology* 22: 847–859. doi:10.1175/JTECH1728.1.

Wyatt, L. R., and J. J. Green. 2009. “Measuring High and Low Waves with HF Radar.” In *Proceedings of OCEAN_EUROPE*, 1–5. Bremen, Germany, May 11–14. doi:10.1109/OCEANSE.2009.5278328.

Wyatt, L. R., J. J. Green, and A. Middleditch. 2011. “HF Radar Data Quality Requirements for Wave Measurement.” *Coastal Engineering* 58: 327–336. doi:10.1016/j.coastaleng.2010.11.005.

Wyatt, L. R., J. J. Green, A. Middleditch, M. D. Moorhead, J. Howarth, M. Holt, and S. Keogh. 2006. “Operational Wave, Current and Wind Measurements with Pisces HF Radar.” *IEEE Journal of Oceanic Engineering* 31 (4): 819–834. doi:10.1109/JOE.2006.888378.

Wyatt, L. R., J. J. Green, K. W. Gurgel, J. C. Nieto Borge, K. Reichert, K. Hessner, H. Günther, et al. 2003. “Validation and Intercomparison of Wave Measurements and Models during the EuroROSE Experiments”. *Coastal Engineering* 48: 1–28. doi: 10.1016/S0378-3839(02)00157-6.

Wyatt, L. R., S. P. Thompson, and R. R. Burton. 1999. “Evaluation of High Frequency Radar Wave Measurement.” *Coastal Engineering* 37: 259–282. doi:10.1016/S0378-3839(99)00029-0.

Zhou, H., and B. Wen. 2015. “Wave Height Extraction from the First-Order Bragg Peaks in High-Frequency Radars.” *IEEE Geoscience and Remote Sensing Letters* 12 (11): 2296–2300. doi:10.1109/LGRS.2015.2472976.

Zhou, H., H. Roarty, and B. Wen. 2015. “Acta Oceanol.” *Sin* 34: 73. doi:10.1007/s13131-015-0599-6.